**Supplemental Material to 'Transient x-ray fragmentation: Probing a prototypical photoinduced ring opening'**

*1. VMI amd TOF detector description.* The VMI detector had an 80 mm diameter MCP (Burle Industries Inc.) and a phosphor screen imaged on to an Opal 1000 camera (with 1024×1024 pixels, each of 5.5×5.5 $\mu$m$^2$ area; manufactured by Adimec). The ion-TOF detector had a 40 mm diameter MCP and was located at a distance of 597.4 mm from the interaction region.

*2. Confirmation of the linear x-ray absorption regime.*

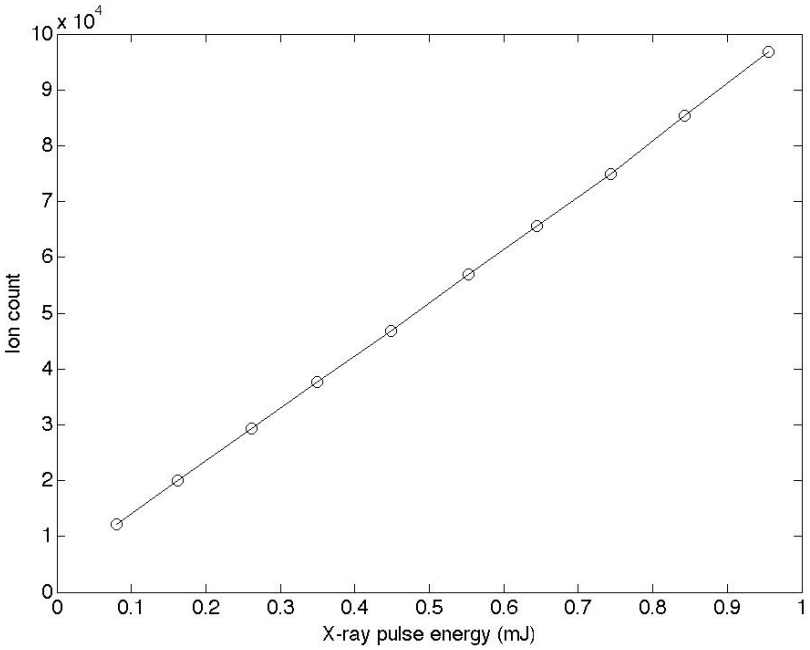


FIG. I. Dependence of the ion-count on the x-ray pulse energy in a UV pump x-ray probe experiment (recorded using the VMI detector). As the x-ray pulse energy fluctuates from shot to shot, all shots were binned into ten energy bins. The average ion count for each bin is plotted vs. the average x-ray pulse energy for that bin. The data were recorded in the presence of the UV pulse, at a fixed delay from the x-ray pulse.

*3. Image processing.* The centering was performed by minimizing the square root of the sum $(Q_1 - Q_2)^2 + (Q_3 - Q_4)^2 + (Q_1 - Q_3)^2 + (Q_2 - Q_4)^2$ for each time bin individually (all centers were in the range of $\langle X_{center} \rangle \pm 6$ pixels, $\langle Y_{center} \rangle \pm 2$ pixels), where $Q_i$ is the number of counts in the $i^{th}$ quadrant in the ring between radii 275 and 325 pixels. Because

of damage to our MCP detector close to its center, only the region outside of the 100-pixel radius, and only one quadrant, was included in the analysis. Outer portion of the data was used for centering for the same reason.

*4. Time evolution of the radial distribution of the ion counts.*

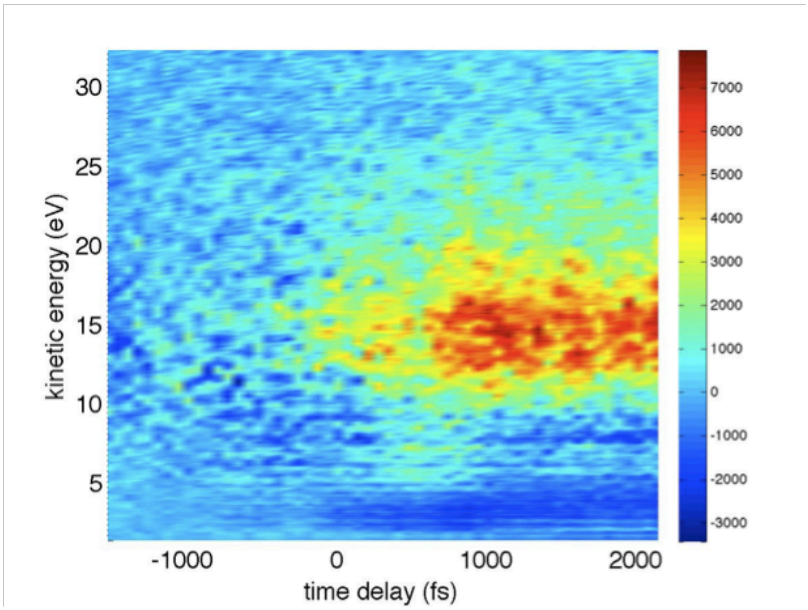


FIG. II. Radial distribution of ion fragments vs. UV-x-ray time delay (after inversion), plotted as a difference relative to the average radial distribution at early time.

*5. Time evolution of the average ion count.*

*6. CHD and HT X-ray fragmentation data from ALS.*

*7. Calculation of the C-H bond length variation upon the UV excitation.* We performed direct *ab initio* excited state dynamics study of 1,3-cyclohexadiene (CHD) in the gas phase using the *ab initio* multiple spawning (AIMS) method. Complete-active-space self-consistent field theory was used to account for the electronic structure. Details of the dynamics are reported elsewhere [5]. Dynamics revealed various conical intersections which are connecting the first three states and responsible for the rapid internal decay, within 300 fs after the UV excitation. The population-weighted average C-H bond lengths were calculated from 80 dynamics simulations. Our calculation indicates that even though the average C-H bond length does decrease upon UV excitation, this would lead to a less than a percent increase in the $H^+$ KER in the first 300 fs, insufficient to fully account for the experimentally observed change in the ion-KER.

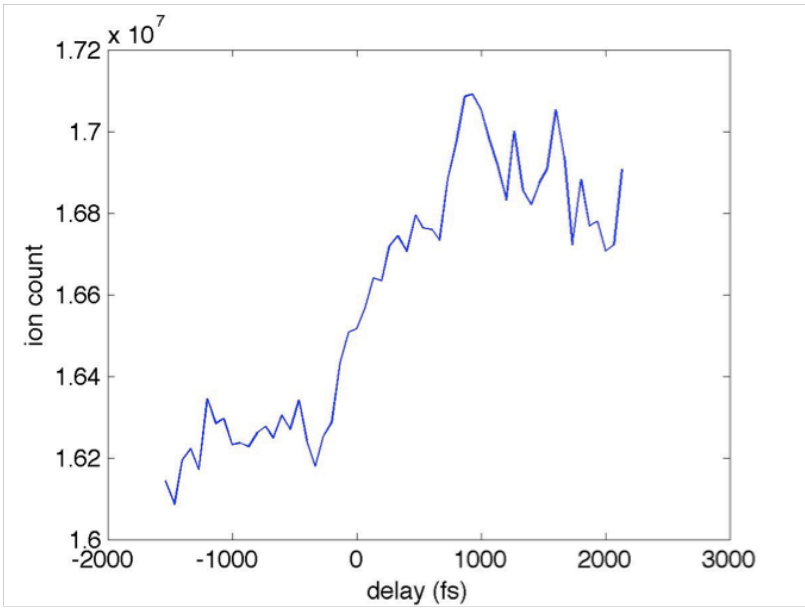


FIG. III. Ion count recorded with the VMI detector, plotted vs. UV-x-ray time delay.

*8. Calculation of the Auger transition intensities.*

The Auger decay rates shown in Fig. V are given by

$$\gamma = \frac{2\pi}{\hbar} \sum_{l_0 m_0} | < \Psi^{(-)}_{\Gamma_0} | \sum_{i \neq j} \frac{e^2}{r_{ij}} | \Phi_0 > |^2 = \frac{2\pi}{\hbar} \sum_{l_0 m_0} |I_{\Gamma_0}|^2, \tag{1}$$

where $\Phi_0$ is the initial core-hole state of the ion, $\Psi^{(-)}_{\Gamma_0}$ is the final continuum state, and $I_{\Gamma_0}$ is the Auger decay amplitude. Note that we use $\Gamma_0$ as a combined index to denote the target electronic state and the angular momentum quantum number $l_0 m_0$ of the ejected electron. In our approach $\Psi^{(-)}_{\Gamma_0}$ is obtained with the complex Kohn variational principle [1], and here we give a brief summary. The final-state wavefunction for production of ions in a specific state $\Gamma_0$ is written as

$$\Psi^{-}_{\Gamma_0} = \sum_{\Gamma} A(\chi_\Gamma F^{-}_{\Gamma\Gamma_0}) \tag{2}$$

where $\Gamma$ labels the final target states $\chi_\Gamma$ included, $F^{-}_{\Gamma\Gamma_0}$ are channel functions that describe the Auger electron, and $A$ is the antisymmetrization operator. In the current application, only one ionic target state is included in the trial wavefunction, that being the final dication state. In the Kohn method the channel functions are further expanded in the molecular

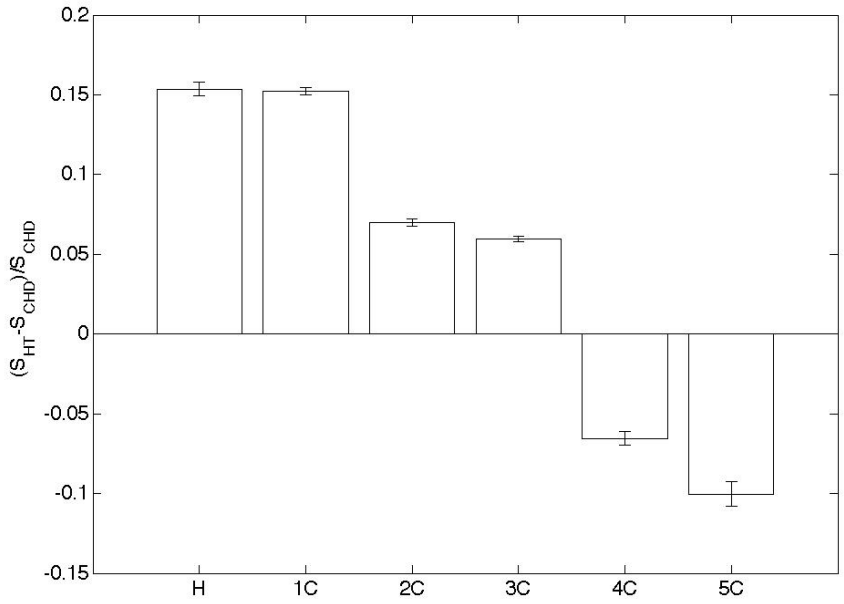


FIG. IV. Relative differences in the ion count between ground-state HT and CHD, recorded at Advanced Light Source at Lawrence Berkeley National Lab. The data are plotted as ($S_{HT}$-$S_{CHD}$)/$S_{CHD}$, where $S_{HT}$ and $S_{CHD}$ are integrated ion counts for HT and CHD, respectively. The results are given separately for different ion groups, such as $H^+$ and $C_nH_m{}^+$, where $n$ is indicated in the figure. Note that a mixture of $t$Z$t$- and $t$E$t$-HT was used in this experiment.

frame as

$$
\begin{aligned}
F^-_{\Gamma\Gamma_0}(\mathbf{r}) = & \sum_i c_i^{\Gamma\Gamma_0}\varphi_i(\mathbf{r}) \\
& + \sum_{lm}\Big[f_{lm}(k_\Gamma,r)\delta_{ll_0}\delta_{mm_0}\delta_{\Gamma\Gamma_0} \\
& + T^{\Gamma\Gamma_0}_{ll_0mm_0}h^-_{lm}(k_\Gamma,r)\Big]Y_{lm}(\hat{\mathbf{r}})/k_\Gamma^{\frac{1}{2}}r\,,
\end{aligned}
\tag{3}
$$

where the $\varphi_i(\mathbf{r})$ are a set of square-integrable (Cartesian Gaussian) functions and the $f_{lm}(k_\Gamma,\mathbf{r})$ and $h^-_{lm}(k_\Gamma,\mathbf{r})$ are numerical continuum functions that behave asymptotically as regular and incoming partial-wave Coulomb functions, rescpectively. $c_i^{\Gamma\Gamma_0}$ and $T^{\Gamma\Gamma_0}_{ll_0mm_0}$, T-matrix elements, are determined variationally. The normalization of the final state is chosen such that the asymptotic form of the outgoing part of the scattered wavefunction is

$$
h^-_{lm}(k_\Gamma,\mathbf{r}) = \sqrt{\frac{2}{\pi k_\Gamma}}exp(i[k_\Gamma r - l\pi/2 + zln(k_\Gamma r)/k_\Gamma + \delta_l]) \tag{4}
$$

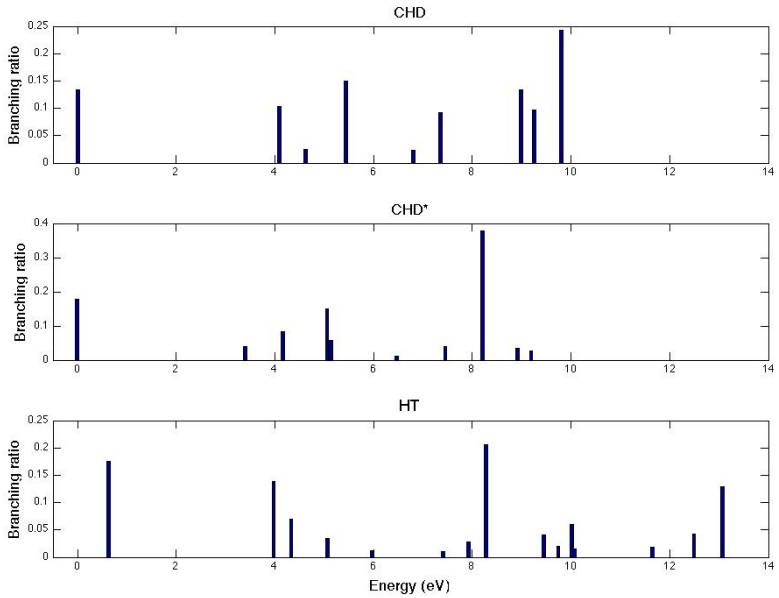


FIG. V. Branching ratio for purely-electronic component of Auger transitions into various dicationic states of CHD, CHD* ($1B_2$), and HT in the ground state CHD and HT geometries, in single-orbital approximation. The excess energy is in each case referenced to the ground state of $CHD^{2+}$ (0.63 eV lower than the ground state of $HT^{2+}$ [6]). This calculation predicts rates more accurately than the energies.

To proceed we consider two cases. (1) Auger electron, $\phi_k$, and the electron that repopulates the core-hole come from the same valence molecular orbital, $\phi_\nu$. (2) The two electrons are from different molecular orbitals, $\phi_\nu$ and $\phi_{\nu\prime}$. The detail derivation can be found in [2], and here we give the final expressions. In case (1) the squared matrix elements for the transition is

$$|I_{\Gamma_0,\nu\nu}|^2 = | < \phi_c(1)\phi_k(2)|\frac{e^2}{r_{12}}|\phi_\nu(1)\phi_\nu(2) > |^2, \tag{5}$$

where $\phi_c$ is the core-hole orbital. In case (2) the amplitudes depend on the spin state of the remaining bound molecule, and the desired matrix elements are

$$\begin{aligned} |I^{sing}_{\Gamma_0,\nu\nu\prime}|^2 &= \frac{1}{2}|J+K|^2 \\ |I^{trip}_{\Gamma_0,\nu\nu\prime}|^2 &= \frac{3}{2}|J-K|^2, \end{aligned} \tag{6}$$

where

$$J =< \phi_c(1)\phi_k(2)|\frac{e^2}{r_{12}}|\phi_\nu(1)\phi_{\nu\prime}(2) >$$
$$K =< \phi_c(1)\phi_k(2)|\frac{e^2}{r_{12}}|\phi_{\nu\prime}(1)\phi_\nu(2) > . \quad (7)$$

All calculations are performed at the equilibrium geometries of neutral CHD and HT, and since Auger decay populates triplet dication states only weakly [2], we only consider decay channels that produce singlet dication states. To avoid working with non-orthogonal orbitals in the calculation, a single set of molecular orbitals is used to construct both $\Phi_0$ and $\Psi^{(-)}_{\Gamma_0}$, and here the orbitals are obtained in the self-consistent Hartree-Fock field of the neutral. Since Auger-electron energy is large, we assume that the orbital relaxation effects are negligibly small [3]. The square-integrable portion of the basis for the complex Kohn calculation consisted of Dunning's double-zeta plus polarization basis [4] for both atoms, and we also included three s-type, two p-type and two d-type functions positioned at the center of mass. The numerical continuum functions up to $l_{max}$ =14 and $m_{max}$=6 are included in the calculation. To determine the relative peak positions in Fig.3 we carried out the complete-active-space self-consistent-field calculation on the dication using 6-31G* basis set.

*9. Momentum change on the CHD$^+$ PES.* We used the *ab initio* molecular dynamics to simulate the core-hole states, by forcing the orbital occupancy of the 1$s$ to be 1 in the electronic structure (Molpro) [7]. Dynamics simulation was performed on the first core-hole state at Hartree-Fock (HF) level for 20 fs with 100 initial conditions sampled from Wigner distribution. The comparison of the averages of the eight C-H bonds lengths over 100 dynamics simulations showed an increase in the C-H bond on the core-excited carbon.

Note a distinction between the C-H bond *increase* discussed here (also referred to in the text of the paper) and the C-H bond *decrease* discussed in the section 7. of the Supplemental Material. The mechanism discussed here does not require UV excitation, and it only pertains to the length(s) of C-H bonds of hydrogen(s) bonded to the carbon that absorbs the x-ray photon. The mechanism discussed in section 7. of the Supplemental Material refers to an average of all C-H bond lengths upon UV excitation to the $1B_2$ state.

*10. Error estimates.* To estimate statistical error in Figures 1, 2 and IV, we randomly divided the data into two sets. In each case both set was subjected to the same processing steps as the complete dataset. Statistical error was extracted from the difference in the

result obtained from the half-datasets compared to the entire dataset.


[1] T. N. Rescigno, B. H. Lengsfield, and C. W. McCurdy, in *Modern Electronic Structure Theory*, edited by D. R. Yarkony (World Scientific, Singapore, 1995), Vol. 1.

[2] H. Siegbahn, L. Asplund, and P. Kelfve, Chem. Phys. Lett. **35**, 330 (1975).

[3] S. K. Semenov, et al., Phys. Rev. A **75**, 032707 (2007).

[4] T. H. Dunning, Journal of Chemical Physics **53**, 2823 (1970).

[5] H. Tao, J. Kim, T. Martinez, J. Chem. Phys.(2012), in preparation.

[6] T. S. Zyubina, et al., Phys. Chem. Chem. Phys. **10**, 2321 (2008).

[7] H. Werner, et al. (2006, see http://www.molpro.net).